Comprehensive Analysis of the Impact of a Novel Droplet Volume Fraction-Based Drag Reduction Correlation in a Numerical Study on Water Sprays with Different Levels of Density

Martin Thielens[a*], Yuanjun Liu[b], Bart Merci[a], Tarek Beji[a]

[a]*Ghent University, Department of Structural Engineering and Building Materials, BELGIUM*

[b]*Wuhan University, School of Civil Engineering, CHINA*

*Corresponding author: Martin.Thielens@ugent.be, ORCID: **0000-0001-7998-2577**

Abstract:

Multiple sets of CFD simulations of water sprays have been carried out with FDS 6.7.6 with a novel expression for the drag reduction model (representing the influence of the surrounding droplets on the drag when compared to the situation for isolated droplets). The sprays are representative for use in fire suppression, but have been characterized in the absence of a fire-driven flow, which is key for a step-wise approach. Previous simulations have shown the importance of the drag reduction model, indicating that for a dense spray, a much stronger significant drag reduction seemed necessary than what is commonly applied, in order to reproduce the measured width of the spray envelope and the subsequent water flux distribution at floor level in the CFD simulations. In the present study, the drag reduction is calculated locally, depending solely on the local droplet volume fraction. It is thus only invoked in the dense region of the spray, typically near the injection. The results reveal very good agreement of the water flux distribution on the ground for the dense spray, with deviations from the experimental results that are less than 4% in the center of spray for the initial mesh. However, the simulation results are sensitive to the mesh size. The novel expression for the drag reduction model has also been tested against two other sprays to evaluate its impact in less dense sprays. The initial set of parameters leads to acceptable simulation results for less dense sprays.

Keywords: Drag Reduction, Water Sprays, CFD

1. Introduction

In fire safety, water sprays from sprinklers or water mist systems are often used as active fire protection systems by, for example, removing heat from the smoke and the flames. The trajectory and the residence time of the droplets in the smoke layer and flame region are of prime importance, as this will define the zone and the time of interaction of the droplet with the surrounding gas. This is derived from the droplet motion, which is governed by gravity and the drag force. It is thus essential in spray modelling to have an accurate estimate of the local drag force.

The drag force depends on the flow regime in the boundary layer of the surrounding gas around the droplet. Therefore, an important non-dimensional number is the droplet Reynolds number (Re_d), which is the ratio of the inertial forces to the viscous forces. The drag coefficient of a single spherical particle as a function of its Reynolds number is relatively well-known and has been extensively investigated. Several correlations may be found in the literature. A brief overview is provided here.

In 1851, Stokes studied the very slow motion of a sphere (a pendulum) in a fluid. He offered an analytical solution for the resistance force from the fluid on the particle [1]. This corresponds to very low Re_d numbers and is known as the Stokes-regime. For this regime, the viscous forces are dominating and no separation of the flow around the sphere is observed. The drag coefficient in this regime is inversely proportional to the Reynolds number [2].

Then for increasing Re_d, the inertial effects become of increasing importance. The flow may begin to separate from the droplet or sphere, from now on called 'particle'. Several experiments investigating the motion of spherical rigid particles in this transition regime have been conducted. In 1940, Lapple and Shepherd compiled experimental measurements of the drag coefficient for spherical particles from 17 different papers and proposed a correlation in [3]. For this transition regime, the correlation between the drag coefficient and the Reynolds number is not simply inversely proportional anymore. Several empirical or semi-empirical formulations have been proposed. A summary of the most popular formulations is provided by Clift *et al.* [4]. These correlations are of different levels of complexity and fit the experimental data more or less accurately. An example is the one provided by Schiller and Naumann, which provides reasonable deviations for $1 < Re_d < 1000$ [5].

For a fully turbulent flow and up to the critical Reynolds number, the wake size and the structure of the flow does not change significantly. Therefore, for the Newton-regime the drag coefficient remains almost constant [2].

Dealing with several particles, and not only isolated particles, increases the level of complexity. Happel highlighted in 1960 that two closely aligned spheres fall faster than an isolated sphere [6]. Even the leading particle is influenced by the trailing particle and falls faster than if it was isolated. This is also confirmed by Chiang and Sirignano who studied the interaction between three identical aligned droplets [7]. They proposed a correction function to compute the drag of each particle. The expression is valid for a spacing between the particles in the range of 2.7 to 12 times the particle diameter and for droplet Reynolds number from 90 to 130. It is clear from the proposed correlations that the drag coefficient of the middle particle (second droplet) is not only influenced by the distance to the leading one (first droplet), but also to the following one (third droplet).

In Computational Fluid Dynamics (CFD) simulations, the size of the particles (and the space between them) is usually too small to be captured on the gas phase mesh. More particularly, in the Lagrangian – Eulerian

approach, the gas phase is considered as a continuum and solved in Eulerian coordinates while the Lagrangian approach is followed for the dispersed phase. This means that these Lagrangian particles are transported in the gas phase and that their impact on the continuous phase is accounted for by the use of source terms in the gas phase equations.

There are different types of interactions between the particles and the fluid, depending on the spray density, as proposed by Elghobashi in 1994 [8].

For very dilute sprays, the distance between the particles is large enough for their effect on the carrier fluid to be negligible. This is known as one-way coupling and is typically valid for a particle volume fraction (α) smaller than 10^{-6}. The particles are too few and too disperse to have a significant influence on the gas phase. Hence, only the continuous phase has an influence on the dispersed phase. In that case, the particles will not influence each other, since the distance between them is very large compared to the size of the droplets.

When the spray density increases, the particles start to have an effect on the gas phase. Thus, not only the carrier fluid has an impact on the particles, but the momentum lost by each particle is also added to the fluid. This is referred to in the literature as two-way coupling [8].

For very dense sprays – typically when the particle volume fraction is above 10^{-3}, the interaction between the individual particles also needs to be taken into account [2]. These interactions may be categorized as direct (collision) or indirect (aerodynamic), as mentioned by Salewski [9]. The first category has already been intensively studied, in contrast to the aerodynamic four-way coupling.

A commonly used correlation [10, 11] for drag reduction is the correlation given by Ramirez [11]. It has been developed for an idealized configuration involving two identical spherical particles placed in tandem, i.e., positioned in line compared to the flow direction, and for a Reynolds number in the order of magnitude of 100. Ramirez provided a correlation for the drag reduction for droplets based on an analytical development of a fully developed wake velocity profile that is fitted by experimental data. This correlation is used in the Fire Dynamics Simulator (FDS) to account for the drag reduction in case of dense sprays [10]. Zhu *et al.* [12] have provided another empirical function for the drag reduction of the trailing particle (the second particle) that is aligned to the leading particle (the first particle). This correlation also depends on the interspacing distance and the Reynolds number. Salewski proposed another correction factor for the drag coefficient, which takes into account the non-alignment of two droplets compared to the main flow direction [9]. In his investigation, the two droplets undergo similar flow conditions and are limited to Re_d of 50, 100 and 200. Prahl *et al.* have conducted numerical work on the interaction between two fixed spherical particles for similar conditions [13] and found that the situation that leads to the highest drag reduction is the tandem arrangement (i.e., when the particles are aligned compared to the flow direction). For this configuration, the drag reduction for the trailing particle, compared to an isolated one, is as high as 60%, 70% and 80% for Re_d= 50, 100 and 200, respectively. It is worth noting that such levels of drag reduction are significantly higher than what is commonly used to date in fire related CFD simulations with water sprays (e.g., [14]). Finally, more complex correction functions are available in the literature, such as in [15] where the proposed function is a combination of two idealized cases, i.e., when the two particles are exactly aligned and when the two particles are exactly aside. Then, two correction functions are used to adjust the drag coefficient due to an azimuthal position (neither exactly upstream nor exactly aside).

A thorough assessment of the drag reduction correlations described above in the context of a full collection of water droplets, i.e., a spray, is very scarce if not inexistent. This is essentially due to the lack of detailed water spray experimental measurements as well as the difficulty to interpret and apply the correlations developed for two or three particles (in idealized conditions) to a full spray.

The present study is motivated by an apparent lack of in-depth assessment of the drag reduction model in CFD simulations of full water sprays typical for fire suppression applications, to the best of the authors' knowledge. To that purpose, multiple water sprays, with variable level of density (or particle volume fraction, α) are investigated: the 'Wuhan' spray [16], the 'VTT' spray [17] as described in the FDS validation guide [18] and the 'Fukui' spray [19]. Based on the operating conditions and the spray characteristics, the Wuhan spray is expected to be much denser than the two other sprays and has been the starting point of this research. However, all the three sprays are important in this initial assessment of the novel Droplet Volume Fraction (DVF-)based drag reduction model.

A novel expression for the reduction of the drag model is introduced, based on correct asymptotic behavior for very dilute and very dense spray, with a smooth transition in between. The impact of the different parameters in the mathematical expression is illustrated.

The initial case for the discussion of the impact of this novel DVF-based drag reduction model on CFD simulations is the Wuhan spray, for which experiments have been carried out in order to characterize the overall shape of a water mist spray and the subsequent water density distribution on the floor [16]. The follow-up comprehensive numerical study carried on in the latter paper has shown that the predicted spray is significantly narrower (by 78%) than the actual spray. This has been explained (for the case at hand) by the fact that the drag is not sufficiently reduced with the model of Ramirez. An ad-hoc approach has been proposed (for solely diagnostic purposes) by setting the drag coefficient to a constant for all droplets and reducing it sufficiently to capture the spray shape correctly.

In this paper, it is therefore intended to present a correlation where the drag is only reduced in sufficiently dense regions of the spray. The approach followed here differs from some of the fundamental studies, e.g., for particles in tandem, described above, in that it is an 'engineering approach' where the correlation is developed based on agreement of CFD simulation results of full sprays with experimental data. Such approach has been carried out in previous studies and in other two-phase flow configurations. For instance, in [20], Rusche *et al.* analyzed the drag force on disperse elements for various two-phase flows (i.e., solid particles in fluid carrier, fluid particles in fluid and gaseous bubbles in liquid carrier). In that paper, some interesting observations that also apply to the case at hand are made: a reduction in drag is applied based on the concentration of the disperse elements only. In [21], a novel drag force model, which takes into account the non-dimensional droplet spacing, has been proposed for diesel sprays. Interestingly and similarly to what is expected for the Wuhan spray (examined in [16]), it has been pointed up in [21] that a drag force reduction tends to increase the spray volume. In addition to [21], the same approach has been followed in 'bubbly flows', e.g., in [22] and [23]. This is a different application yet with interesting similar features that will be pointed at during the discussion of the proposed drag reduction model. Whereas, as mentioned, agreement with experimental data is an important aspect, it is worth mentioning that the novel expression for the drag reduction will respect asymptotic behavior for very dilute and very dense sprays as well.

2. Numerical Modeling

The Computational Fluid Dynamics (CFD) package Fire Dynamics Simulator (FDS 6.7.6), developed by the National Institute of Standards and Technology (NIST), is used in the present study. Turbulence is solved using Large Eddy Simulation (LES). The gas phase is solved in the Eulerian coordinates while the particles are tracked in a Lagrangian manner. Only the most relevant equations are provided in this paper. More details are found in [10].

2.1. Momentum transfer

If only the drag and the buoyancy forces are taken into account, the momentum equation for a droplet reads:

$$\frac{d(m_d\overrightarrow{U_d})}{dt}=\frac{1}{2}C_D\rho_g A_{d,c}(\overrightarrow{U_g}-\overrightarrow{U_d})^2\frac{\overrightarrow{U_g}-\overrightarrow{U_d}}{\left\|\overrightarrow{U_g}-\overrightarrow{U_d}\right\|}+V_d(\rho_l-\rho_g)\vec{g} \quad (1)$$

where m_d, U_d, $A_{d,c}$, V_d and ρ_l are, respectively, the mass, the velocity, the cross-sectional area, the volume and the density of the droplet. As the droplet is assumed to be spherical, $m_d=\rho_l V_d$, $A_{d,c}=\pi\, d^2/4$ and $V_d=\pi\, d^3/6$. The variables t, C_D, ρ_g, U_g and g denote, respectively, the time, the drag coefficient, the density of the surrounding gas, the velocity of the gas and the gravitational acceleration.

For a non-evaporating droplet, equation (1) can be simplified as:

$$\frac{d(\overrightarrow{U_d})}{dt}=\frac{3}{4}C_D\frac{\rho_g}{\rho_l}\frac{1}{d}\overrightarrow{U_r}^2\frac{\overrightarrow{U_r}}{\left\|\overrightarrow{U_r}\right\|}+\frac{(\rho_l-\rho_g)}{\rho_l}\vec{g} \quad (2)$$

where $\vec{U}_r=\vec{U}_g-\vec{U}_d$ and d is the droplet diameter.

2.2. Drag coefficient of an isolated droplet

As mentioned in the introduction, the drag force depends on the flow regime in the boundary layer of the surrounding gas around the droplet. An important non-dimensional number that describes the flow regime around the spherical droplet is the droplet Reynolds number:

$$\mathrm{Re}_d=\frac{\rho_g\, d\left\|\overrightarrow{U_g}-\overrightarrow{U_d}\right\|}{\mu_g} \quad (3)$$

with d the particle diameter and $\mu_g$the dynamic viscosity of the gas.

In FDS [10], the expression for the drag coefficient of one single spherical droplet is a combination of three correlations that depend on the flow regime:

$$C_{D0} = \begin{cases} \dfrac{24}{\mathrm{Re}_d} & \mathrm{Re}_d < 1 \\ \dfrac{24}{\mathrm{Re}_d}\left(0.85 + 0.15\,\mathrm{Re}_d^{\,0.687} \right) & 1 < \mathrm{Re}_d < 1000 \\ 0.44 & 1000 < \mathrm{Re}_d \end{cases} \quad (4)$$

The first line provides a correlation that is valid for the Stokes regime. The second line is the correlation proposed by Naumann [24] and finally, for high Reynolds numbers, a constant value is used for very turbulent flows.

2.3. Drag reduction

In the correlation of Ramirez [11], used in [10], the drag coefficient of the trailing sphere reads :

$$C_D = C_{D0}\frac{F_D}{F_{D0}} \quad (5)$$

where C_{D0} is the drag coefficient of the corresponding isolated particle and F_D/F_{D0} is the hydrodynamic force ratio on the trailing droplet, computed as:

$$\frac{F_D}{F_{D0}} = W\left[1 + \frac{\mathrm{Re}_d}{16}\frac{1}{(L/d - 1/2)^2}\exp\left(-\frac{\mathrm{Re}_d}{16}\frac{1}{(L/d - 1/2)} \right) \right] \quad (6)$$

where L is the distance between the center of the two droplets. Moreover, W is the dimensionless local wake velocity of the trailing sphere which is induced by the leading droplet, i.e.:

$$W = 1 - \frac{C_{D0}}{2}\left[1 - \exp\left(-\frac{\mathrm{Re}_d}{16}\frac{1}{(L/d - 1/2)} \right) \right] \quad (7)$$

Equations (6) and (7) are invoked in FDS when the local volume fraction, α, exceeds 10^{-5} [14]. The latter is linked to the non-dimensional distance between the two droplets: $L/d = \left(\frac{\pi}{6}\alpha \right)^{\frac{1}{3}}$ ([2], [16]).

It is worth mentioning that Ramirez's correlation is only valid when the distance between the two droplets is not too small, as the correlation is developed based on the velocity profile of a fully developed axisymmetric wake behind the leading particle. For smaller particle-to-particle distance, the drag reduction is underestimated [13]. Furthermore, this correlation has been developed for a particle Reynolds number between 24 and 130.

An alternative to the correlation of Ramirez for the drag reduction (and which is examined in this work) is the empirical function from Zhu [12]:

$$\frac{F_D}{F_{D0}} = 1-(1-A)\exp\left(\quad B\frac{L}{d} \quad \right) \qquad (8)$$

where

$$A = 1-\exp(-0.483+3.45\times10^{-3}\,\mathrm{Re}_d-1.07\times10^{-5}\,\mathrm{Re}_d^{\,2}) \qquad (9)$$

$$B = -0.115-8.75\times10^{-4}\,\mathrm{Re}_d+5.61\times10^{-7}\,\mathrm{Re}_d^{\,2} \qquad (10)$$

This formulation has also been developed for the particular configuration of two aligned particles. This correlation is valid for Re_d ranging from 20 to 150 and depends, as the Ramirez equation, only on the Reynolds number and the interspacing distance.

2.4. Novel Droplet Volume Fraction-based drag reduction model

A novel expression for the drag reduction is developed in order to further increase drag reduction, in comparison to the previously tested models, to provide simulation results that are closer to the experimental ones.

The experimental data set from Zhu [12] shows that for $54 < Re < 145$ the drag ratio, F_D/F_{D0}, does not vary substantially. It was thus decided to first develop a model that would only depend on the droplet volume fraction (as done in [20]), and not the Reynolds number.

This function first of all needs to be consistent with certain conditions. The first one is that for very dilute sprays (very low droplet volume fraction) there should be no drag reduction as the inter droplet distance is so large that there are no interactions between particles. In other words, for low α, $f(\alpha)$ should be $f(\alpha) = 1$. Secondly, it was decided to set the drag reduction to a constant value once α exceeds a certain threshold value, as advocated in [22, 23] for bubbly flows. Indeed, in [22], McClure *et al*. indicate that above a certain volume fraction (0.10 to 0.20) the value of the correction function may be regarded as essentially constant. Similarly, Rabha found that above a certain value, the effect of the volume fraction on the velocity (and thus the drag coefficient) diminishes [23]. He suggested that this phenomenon is due to an increased lateral interaction between the bubble that takes over the wake effect induced by the leading bubbles.

Based on the above, the following equation is proposed:

$$\frac{F_D}{F_{D0}} = (1-B)\exp\left[\quad -\left(\quad \alpha+1-A \quad \right)^n \quad \right]+B \qquad (11)$$

where A, B and n are parameters of the function and α is the local droplet volume fraction.

This mathematical expression proposed for the novel approach is believed to be suited for the problem at hand as it is very easy to adjust and control the shape of the curve thanks to the three parameters. For instance, the parameter A will determine around which value of α the transition will occur. An increase of this parameter will translate the transition region horizontally (see Figure 1). Then the maximum value of the drag reduction correction that will be applied for the very dense regions of the spray is determined by the parameter B. An increase of this parameter will simply translate vertically the bottom plateau to

the new value of B. Finally, the parameter n will fix the transition between the region with no reduction ($F_D/F_{D0} = 1$) and with the maximum correction factor ($F_D/F_{D0} = B$). The parameter n will thus determine how those two regions are linked. A decrease of n will decrease the slope and lead to a smoother transition.

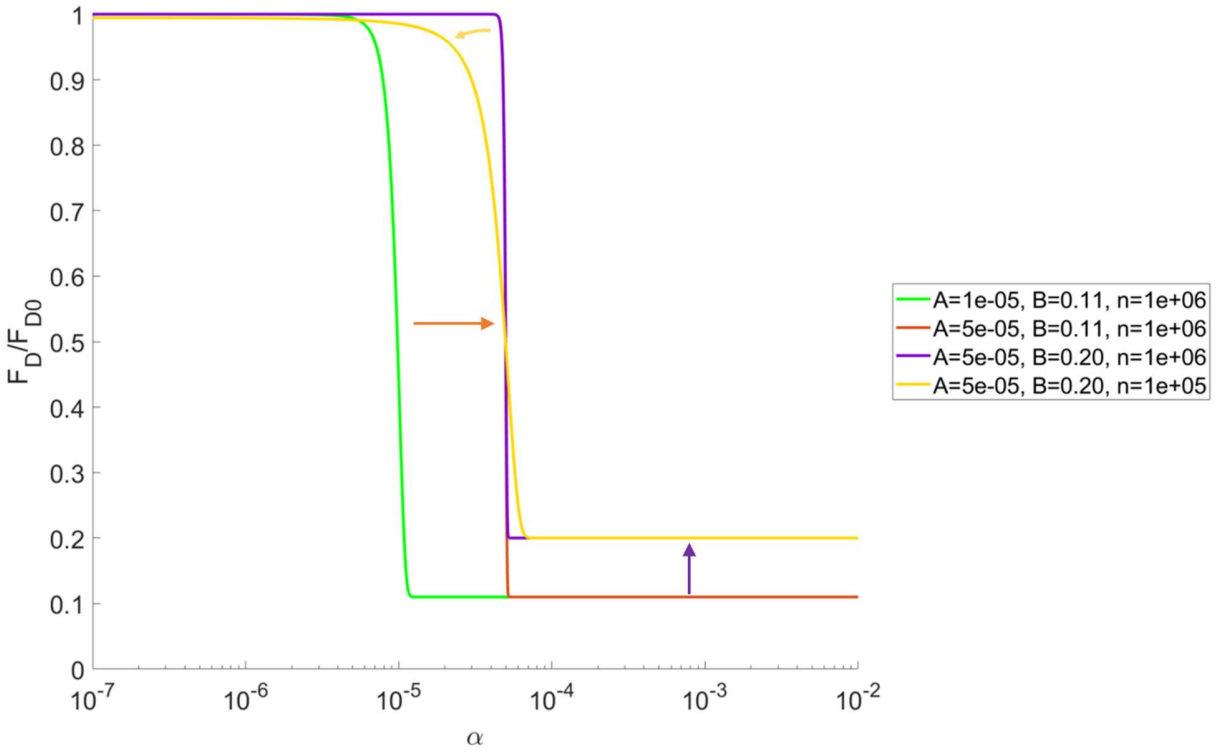

Figure 1 – Illustration of the influence of the parameters A, B & n on the shape of the curve of the novel model

After some simulations, it was decided to set the value of A to 5×10^{-5}. This is higher than the critical value of 10^{-5} chosen in FDS (below which no drag reduction is applied). In order to have an idea of the value of the parameter B that needs to be taken in this model, the FDS source code has been slightly modified. At each time step, a certain percentage of the normally computed drag coefficient is taken by adding a line at the end of the drag subroutine, changing C_D into xC_D with $0 < x < 1$ a parameter that stands for the reduction applied. This approach cannot be generalized and is not based on scientific reasoning. Indeed, this drag reduction will be applied everywhere in the spray, even in the very dilute regions. Hence, these simulations (not shown here) are used only to provide an insight for the value of B that needs to be reached in the dense regions of the spray. They indicate that a value x in the order of 0.2 leads to simulation results that are close the experimental results for the 'Wuhan' spray. After different sets of simulations with different parameters, the value of B has been set to 0.11.

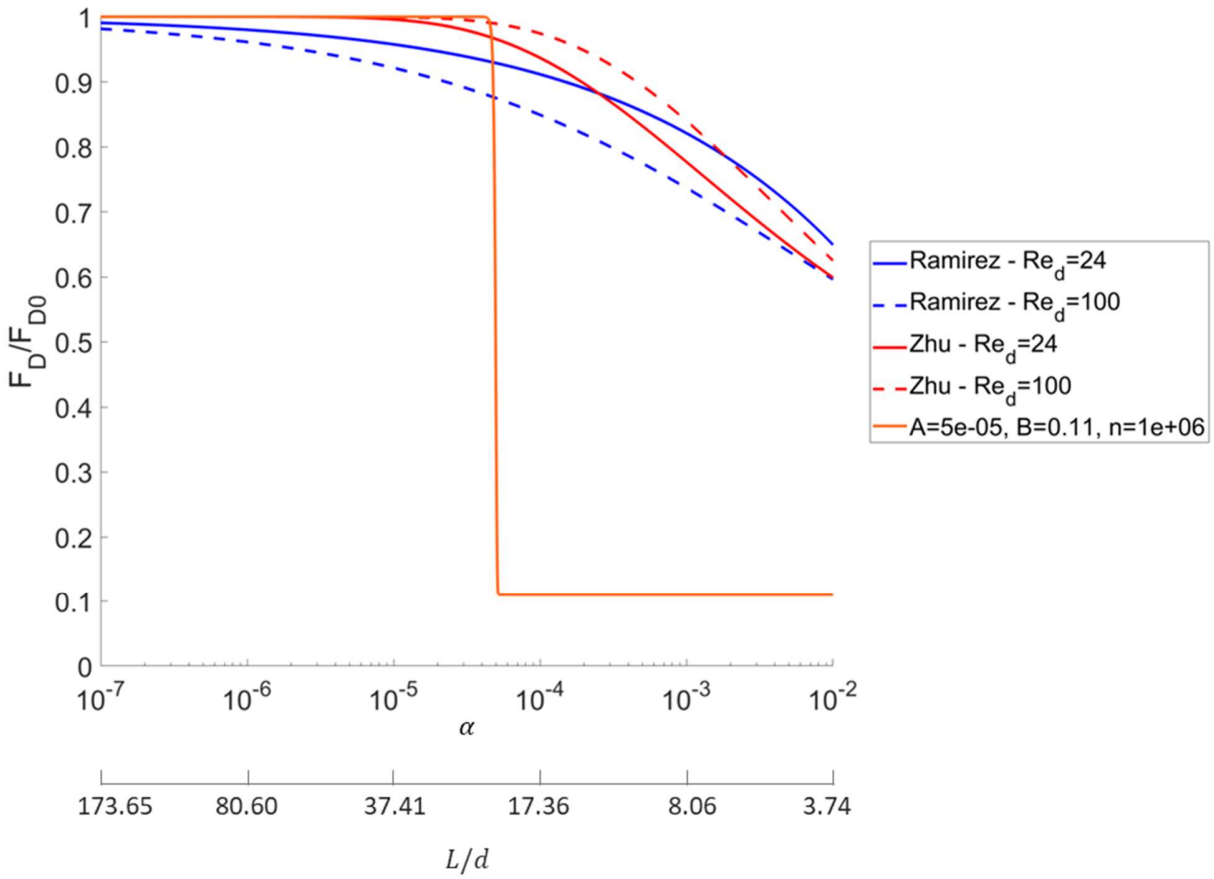

Figure 2 – Illustration of different drag reduction functions as a function of the droplet volume fraction and the adimensional inter-particle distance

A graphical representation of the novel DVF-based drag reduction function is proposed in orange on Figure 2 for the following combination of parameters: $A = 5 \times 10^{-5}$, $B = 0.11$ and $n = 10^6$. The choice for the values of A and n is discussed below. The drag correction reaches 50% for $\alpha = 4.98 \times 10^{-5}$, i.e. very close to the value of A. Note that the x-axis is logarithmic to cover all the very dilute and super dense regions in a spray. As wanted, the novel curve leads to a more important drag reduction for the dense regions of the spray than the Ramirez equation. It is assumed that coalescence does not occur in the sprays considered in this paper. Therefore, the potential effect of large droplets, resulting from coalescence at very high droplet volume fraction, which may behave differently than small droplets is not considered in the present study.

3. Results and discussion for the Wuhan spray

3.1. Experimental setup and measurement techniques of the Wuhan spray

The experimental results obtained by Liu *et al.* and described in [16] are used as initial case in this paper ('Wuhan' spray). A single water mist nozzle is placed at a height of 2.2m in a reduced-scale tunnel. The nozzle operates at a pressure of 1.0 MPa and provides a water flow rate of 1.0 L/min. A laser sheet, used to visualize the overall shape of the spray, shows that the spray exhibits a conical shape near the nozzle (with an angle of 42°) and then becomes a cylinder where the gravitational force becomes dominant. Liu

finds that the maximum cone diameter is around 1.26 ± 0.18m and the cone height from the orifice is 0.7 ± 0.1m (see Figure 3).

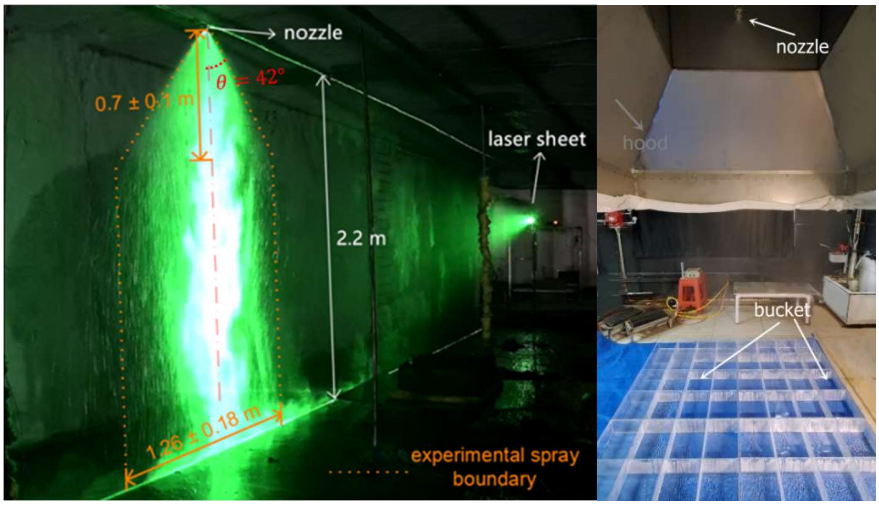

Figure 3 – Left : Laser sheet visualization of the water mist (from [16], with minor modifications), Right : Experimental configuration in open space [16]

The droplet size distribution (DSD) has also been measured based on NFPA 750 [25]. It was found that the measured cumulative mass fraction fits a Rosin-Rammler-lognormal distribution with a volume-median diameter, $D_{V,0.50}$, of $90\ \mu m$, and a spread factor, γ_D, of 6.4.

The water flux density distribution has been obtained by conducting two bucket tests in an open space, see Figure 3 (right). The water mist nozzle was placed inside a hood at 2.2 m height. Below, at floor level, 8×8 buckets were placed. Each squared bucket had an area of $A_0 = 0.2\ \mathrm{m} \times 0.2\ \mathrm{m} = 0.04\ \mathrm{m}^2$. The resulting average water flux as a function of the radial distance, including mean values and standard deviations, is displayed in Figure 4.

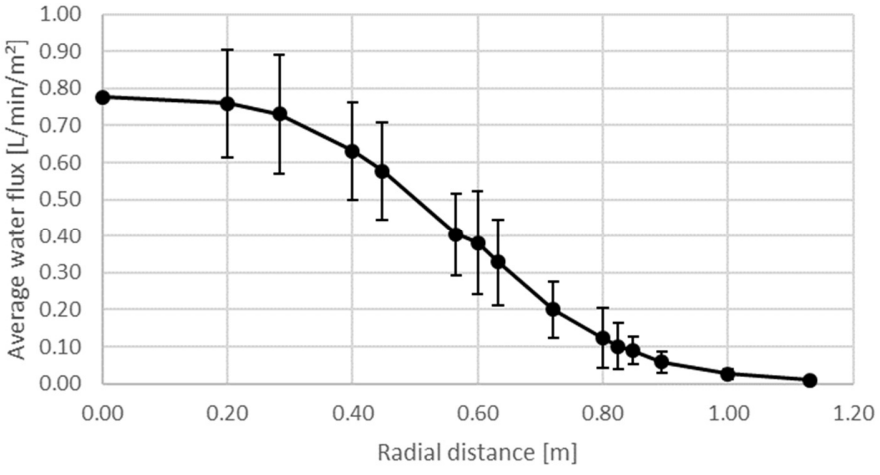

Figure 4 – Experimental average water flux density on the floor as function of the radial distance from the nozzle head for the Wuhan spray. Bars indicate standard deviations.

It is worth mentioning that an extensive sensitivity analysis has been conducted on the choice of the parameters A, B and n. These parameters have been obtained based on a calibration using the specific water spray at hand and a pre-defined cell size. In the remainder of the paper, a mesh sensitivity analysis is carried out in order to examine the potential effect on the water volume fraction and the subsequent 'optimum' values of A, B and n. Then, other sprays will be considered in order to assess the effect of the novel DVF-based drag reduction model on the droplet dynamics under operating conditions (e.g., water flow rate, angle, droplet diameter…etc.) that are different from the Wuhan spray. The following section will start with the default version of the FDS code that will be used as a reference point for the analysis.

3.2. Default FDS simulation

The initial simulation of the Wuhan spray is very similar to the one presented in [16]. The nozzle is located 60 mm below the ceiling, as in the experiments. The flow rate of the spray is set to 1 L/min and the Droplet Size Distribution mentioned above is prescribed in the simulations. The spray half-angle is imposed as measured experimentally, i.e., θ = 42°. The initial droplet velocity is set to 20 m/s. In the present simulations, the mass flux distribution at the injection boundary (0.001 m from the nozzle) is set to be 'UNIFORM'. An injection rate of 200 000 computational droplets per second is used here (as done in [16]). The default drag reduction model of Ramirez is employed here.

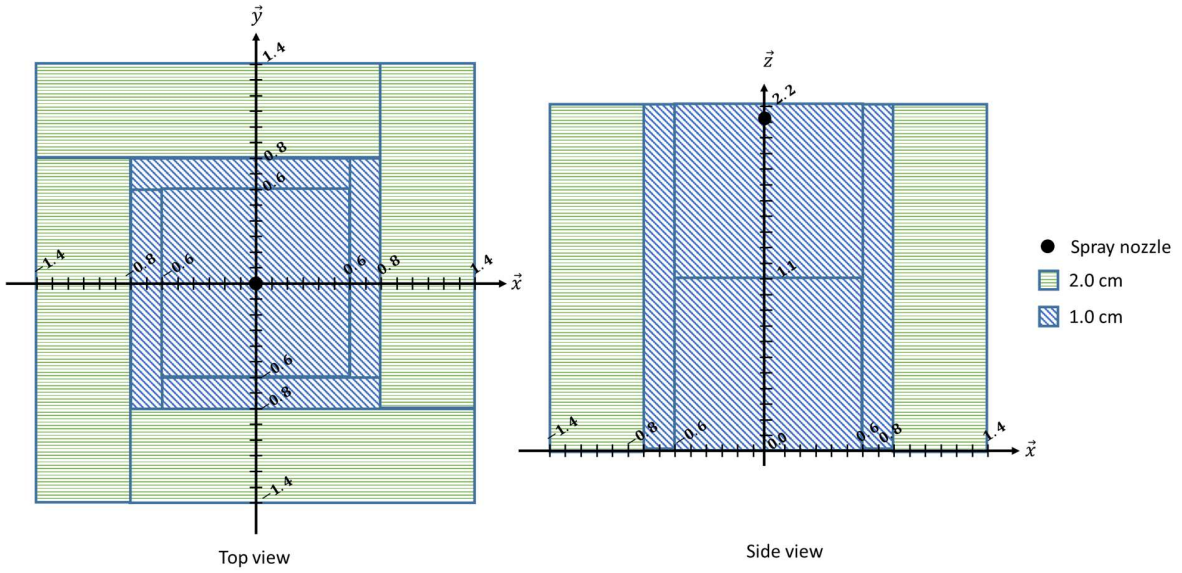

Figure 5 – Mesh for the '1cm simulation' cases for the Wuhan spray

The domain is a rectangular box of size 2.8m x 2.8m x 2.2m. The boundary condition on the sides is set to 'OPEN'. The domain is even wider than in [16] in order to further minimize the effect of the latter on air entrainment around the spray. The domain has been split into multiple meshes in order to resort to parallel computing and reduce the computational time. Special care has been devoted to the design of the mesh (see Figure 5). More particularly, no mesh interface boundary is located in the very core region of the spray, which is enclosed in a single mesh that is centered around the nozzle. In order to optimize the computational cost, only the critical regions of the flow are refined with a maximum ratio of 2:1 at the mesh interface boundaries. The central mesh is now made of cubic cells of 1 cm width and has been split

in two, based on its height, in order to keep an 'acceptable' number of cells per mesh. Around the central mesh, four 1 cm meshes are defined to make the transition to the 2 cm meshes. There are 7 212 800 cells, which is much less than the 1.8×10^7 cells that a conventional uniform mesh strategy would have given. Moreover, with this mesh configuration the entire spray is almost totally captured by the 1cm³ cells.

Regarding the post-processing, the buckets are mimicked using the quantity 'AMPUA' on the 'DEVC' line. The Accumulated Mass Per Unit Area (in kg/m²) was integrated on a surface of 20 cm x 20 cm using the statistics 'SURFACE INTEGRAL' as this corresponds to the collecting area of one bucket. Then, the average water flux density, in $L/m^2/min$, is calculated (similarly to the experiments) as:

$$\overline{\dot{q}''} = 60 \times \frac{\left(\Phi_{t_2} - \Phi_{t_1} \right)}{\rho \times \left(t_2 - t_1 \right)} \qquad (12)$$

where Φ is the AMPUA (in kg/m^2), ρ the water density (in kg/L) and $t_2 - t_1$ is a steady time period which is taken as the last 8 s of the simulation.

As shown in Figure 6 (left), and similarly to the observations reported in [16] for the default case, the predicted spray is too narrow compared to the actual spray. As a consequence, the predicted water flux at the center of the spray at floor level is about 4 times higher than the experimental value, see Figure 7 (left). Further than 0.4 m from the center, the water flux is significantly underestimated, see Figure 7.

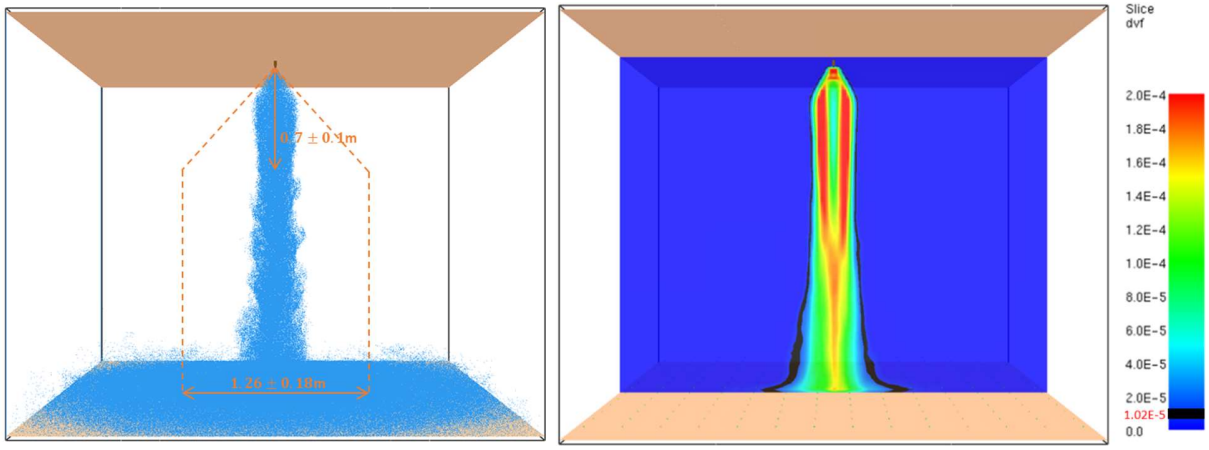

Figure 6 – Left : Spray visualization for the default case and the experimentally observed spray envelope (orange) Right : Time averaged α (on a period of 5s) for the default simulation of the Wuhan spray

Figure 6 (right) displays the droplet volume fraction (α) distribution in the spray (at the center plane). It is worth mentioning that in order to compare the different graphs together, the maximum value has been truncated to 2×10^{-4} on the different visualizations of α in this work. It is clear that the volume fraction is, in most regions, higher than 10^{-5} (this value is marked in black on the Figure), which has been set as a threshold in FDS in order to activate the drag reduction model of Ramirez. However, the effect of the latter for the case at hand appears to be marginal, given that turning it off yields very similar results (not shown here). A similar observation has also been reported in [26] where other water sprays have been studied. For those sprays, Sikanen *et al.* concluded that the droplet-droplet interactions were not important in the modelling of the sprays as turning off this model had only a marginal impact on the results because the spray they investigated was not dense enough. Nevertheless, for the case at hand, it

is believed that the marginal effect of the Ramirez correlation on drag reduction in the dense parts of the spray caused the spray to be too narrow in the CFD simulations. This is illustrated through the impact of the novel expression next.

A second simulation has been run using the correlation of Zhu, Eq. (8), which has been implemented in the source code of FDS 6.7.6.

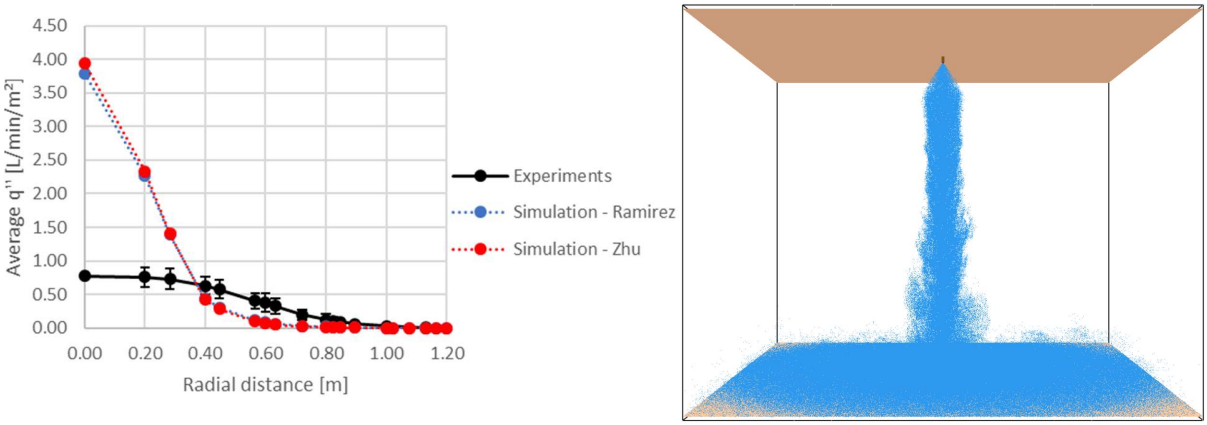

Figure 7 – Left : the water flux density distribution along the radial direction for the default simulation, the Zhu simulation and the experiments of the Wuhan spray and Right : the spray visualization of the Zhu simulation

Once again, the spray envelope is not well captured and is too narrow compared to the experimental observations (Figure 7). The water flux distribution along the radial direction for this simulation is very similar to the water flux distribution for the default case and consequently does not correspond to the footprint of water at ground level obtained with the buckets.

These results indicate that the correlations of Ramirez and Zhu, which have been developed under specific 'idealized' conditions, may not reduce the drag force sufficiently in a full spray, involving many droplets of different sizes and positioned with respect to each other in an 'unorderly' manner.

3.3. Simulation results with the novel DVF-based drag reduction model

The effect of the implementation of the novel expression (Eq. (11)) in the source code has been investigated for the following combination of parameters : $A = 5 \times 10^{-5}$, $B = 0.11$ and $n = 10^6$.

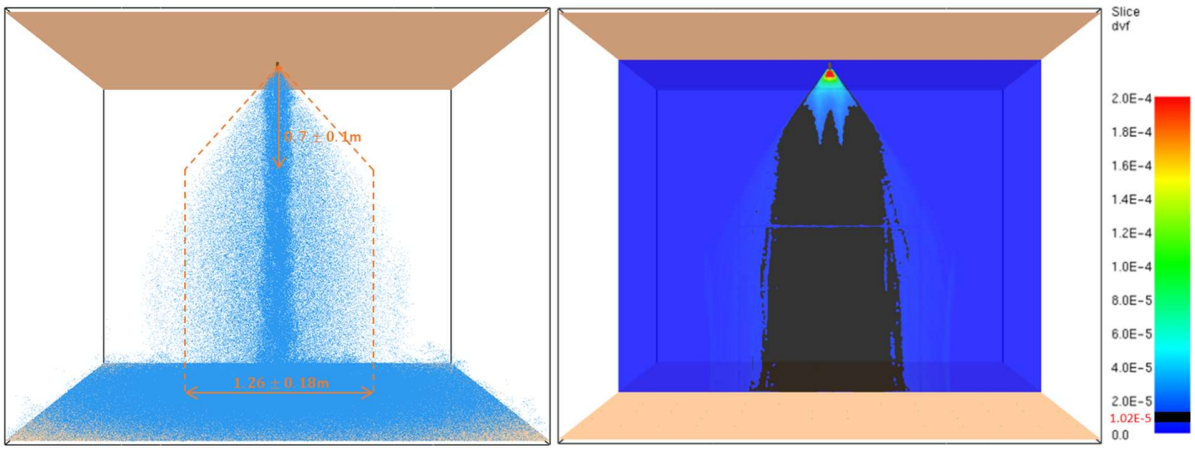

Figure 8 – Left : Spray visualization for the novel model case and the experimentally observed spray envelope (orange) for the Wuhan spray and Right : Time averaged (on a period of 5s) droplet volume fraction for the simulation with the novel DVF-based drag reduction model

The results are displayed in Figure 8 (left) and Figure 9, illustrating that the spray envelope and water flux distribution at the floor agree much better with the experimental data. Even better agreement is possible for this spray through (fine)tuning of the parameters, but this set has been chosen in order to get reasonable agreement with the two other sprays that will be described below.

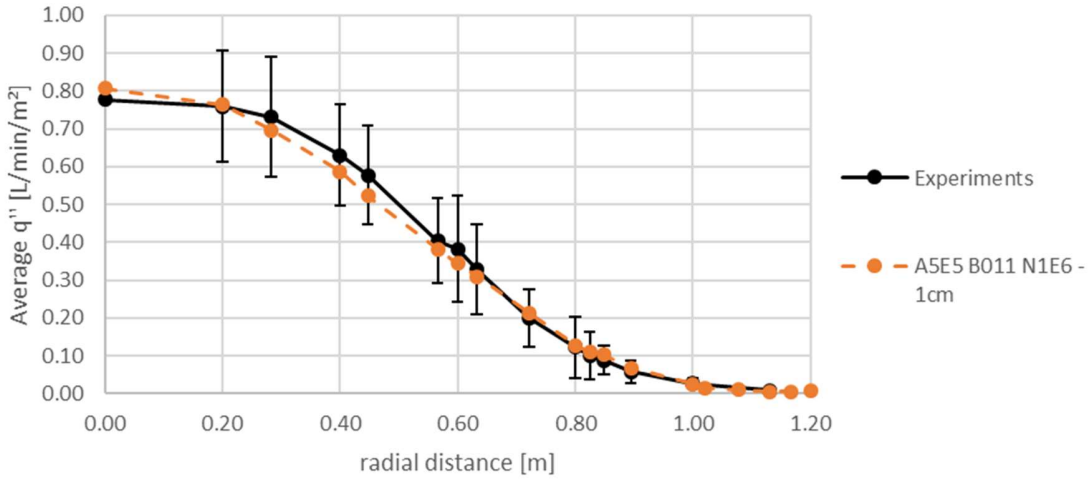

Figure 9 – The water flux density distribution along the radial direction for the novel model drag reduction simulation ($A = 5 \times 10^{-5}, B = 0.11, n = 10^6$) and the experiments for the Wuhan spray

Figure 8 (right) shows that the spray is very dense near the nozzle with a droplet volume fraction that locally even exceeds 2×10^{-4}. Due to the significant drag reduction of 89% with the novel model in this very dense region, the spray is much wider in comparison to the default case simulation. As a consequence, it is also much more dilute in its core region than with the default FDS code. The drag reduction ratio of 11% occurs over a large part of the spray. Indeed, even for $\alpha = 5.2 \times 10^{-5}$ the ratio $F_D/F_{D0} = 0.11$. The region with a droplet volume fraction of 10^{-5} has been highlighted in black on this figure. For this α, the ratio F_D/F_{D0} is 1. So, for an important part of the region, the drag reduction is almost no present.

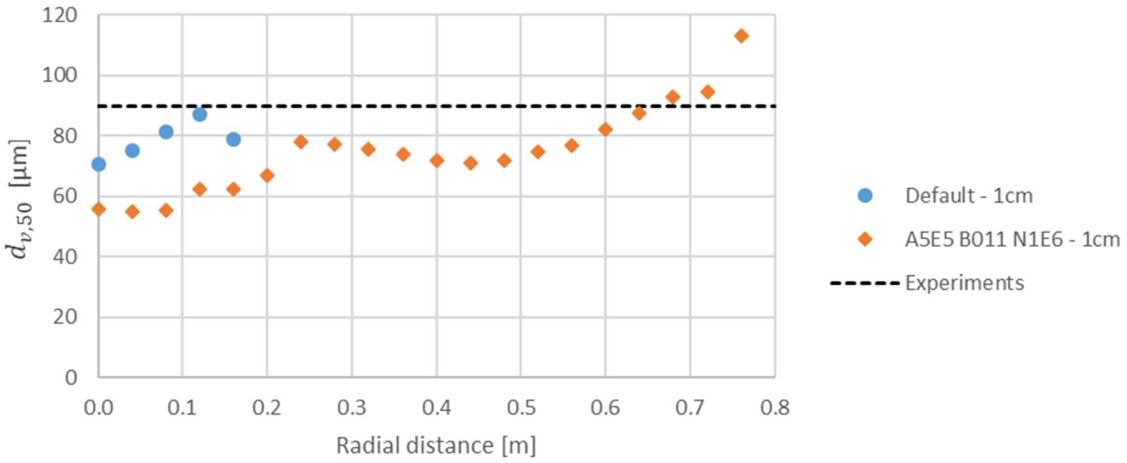

Figure 10 – Simulation results of $d_{v,50}$ at measurements points, every 40 mm, 1 m below the nozzle.

Figure 10 shows the radial evolution of the volume median diameter $d_{v,50}$ at 1 m below the spray nozzle for both the default FDS simulations and the novel DVF-based drag reduction model. These data have been post-processed using PDPA devices in FDS that were placed every 40 mm in each simulation. Regarding the default FDS results, it may be observed that the $d_{v,0.50}$ increases as the radial distance increases (except for the last point on the graph that is close to the edge region of the spray at that height) and is close to the volume median diameter of 90 µm measured experimentally [16]. The same general trend may be observed for the simulation results where the novel DVF-based model is implemented : the volume median diameter increases as the distance to the center of spray increases. Still, it is worth mentioning that, as the spray is already wider at that height and as the biggest droplets are spread more to the edge of the spray, the values of the $d_{v,0.50}$ near the center are lower than for the default simulation.

3.4. Numerical aspects

A mesh sensitivity analysis has been carried out in order to see the impact of this numerical aspects on the simulation results of the novel approach. Two other mesh designs have been investigated.

A cell width of 2 cm everywhere in the domain, that is the cell size that was used in [16] for the Wuhan spray, has been examined. Even if the mesh was broader, a special care has been devoted to this configuration. More particularly, no mesh interface boundary is located in the very core region of the spray, which is enclosed in a single mesh that is centered around the nozzle. The rest of the domain is then split into 4 identical meshes. All meshes have a similar number of cubic cells (432 000 for the center mesh and 448 000 for the others) in order to optimize the running time (see Figure 11).

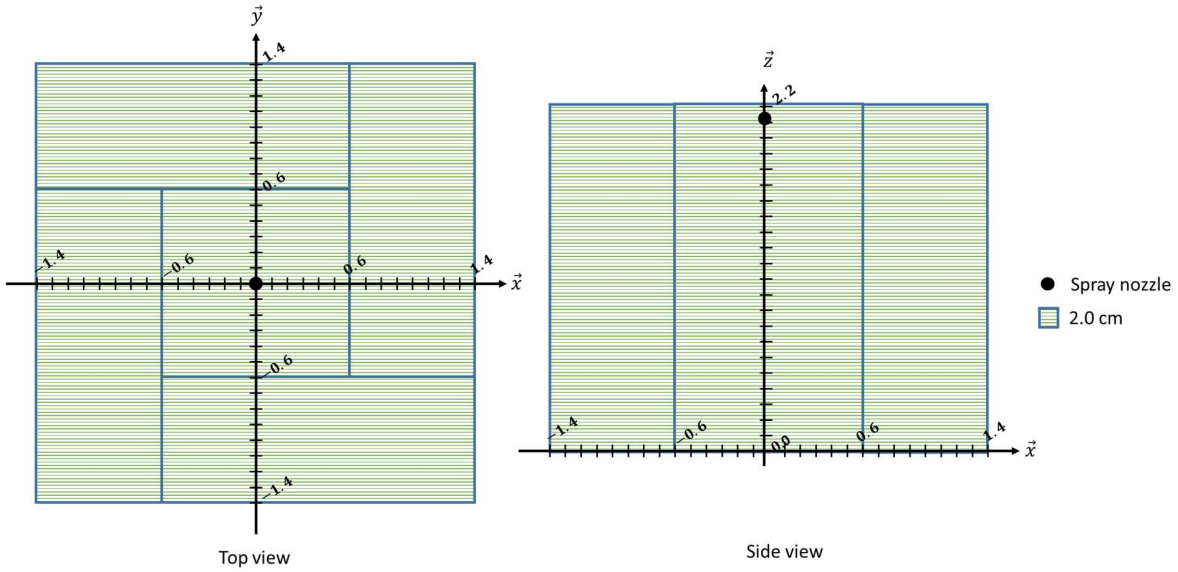

Figure 11 – Mesh for the '2 cm' simulations of the Wuhan spray

The second design is a refinement of the initial mesh configuration. It follows a similar strategy, i.e. the top center part of the spray is again refined (see Figure 12). This region of the spray will indeed define the opening of the spray and therefore impact the footprint of the water spray on the ground floor which is of prime interest in the present paper. In this region, the cell size is again divided by 2 in each direction. Only the top part of the spray has been further refined to avoid a too high number of cells. With this strategy, the number of cells already reaches 1.85×10^7 which, coupled with a number of 200 000 computational particles, leads to a total CPU of around 204 h. The 1 cm³ mesh that can be seen on the top view of Figure 12, also serves to ensure a 'smooth' transition between the very fine mesh and the coarser mesh (by keeping a maximum refinement of 2:1 at the different interface boundaries).

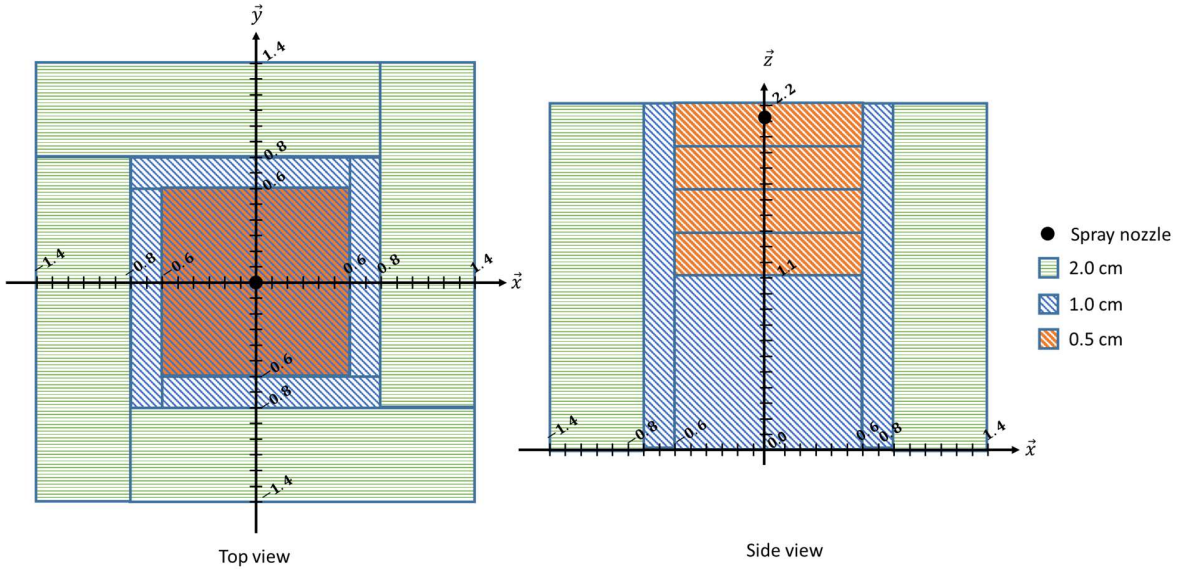

Figure 12 – Mesh refinement strategy for the '0.5cm simulation' cases for the Wuhan spray

The predicted water flux density profiles (for the default FDS simulations with the Ramirez function, and for the CFD simulations using the novel DVF-based drag reduction model) displayed in Figure 13 reveal a significant mesh sensitivity of the results with the novel DVF-based drag reduction expression. In other words, the choice of 'optimum' parameters A, B and n strongly depends on the cell size.

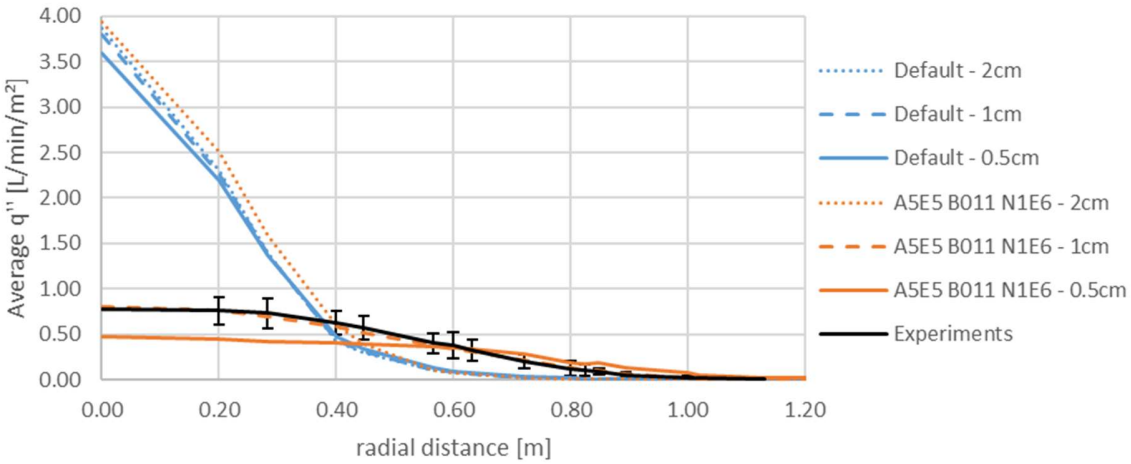

Figure 13 – The water flux density distribution along the radial direction for the Wuhan spray for the default FDS simulations, the novel model drag reduction simulation ($A = 5 \times 10^{-5}, B = 0.11, n = 10^6$) and the experiments

The mesh sensitivity is much less pronounced in the default FDS simulations. This is not surprising, given the very small variation of the drag reduction with α (Figure 2). Whereas less mesh sensitivity may be considered an asset of a model (and vice versa, strong mesh sensitivity can be considered a handicap), it should be acknowledged that the reduced mesh sensitivity is achieved at the cost of an under-predicted reduction in the drag force in very dense regions, which is not a good reason. At present, no optimum has been found, incorporating stronger drag force reduction in a mesh insensitive manner. This is left for future work. It is merely noted here that the introduction of a stronger drag reduction as function of alpha seems to inevitably induce stronger mesh sensitivity, while it is not straightforward to analyze this step by step: the drag reduction affects the flow, and thus the positions, of the particles, which then has a consequence on the local droplet volume fraction α and thus on the drag reduction. On a finer mesh, there is more resolution in the α field and thus the impact of the drag reduction as described, can be affected much more significantly than is the case when α hardly affects the drag reduction.

Figure 14 shows the differences between the different mesh configurations for the default FDS simulations and the novel model simulations. In the simulations with the novel model, the spray is narrower on the 2 cm mesh than with the 1 cm and 0.5 cm meshes. As a consequence, the droplet volume fraction in the spray is on average higher, as the same amount of water is present in a smaller volume. The higher values of α should lead to more drag reduction for the entire spray, but this is not observed in Figure 14. A possible explanation may be that: in the absence of significant drag reduction, the spray remains narrow despite the high droplet volume fraction. With stronger drag reduction, the spray becomes wider and consequently the droplet volume fraction is reduced on average, leading to less drag reduction again (Figure 1). Thus, there is a certain level of internal compensation.

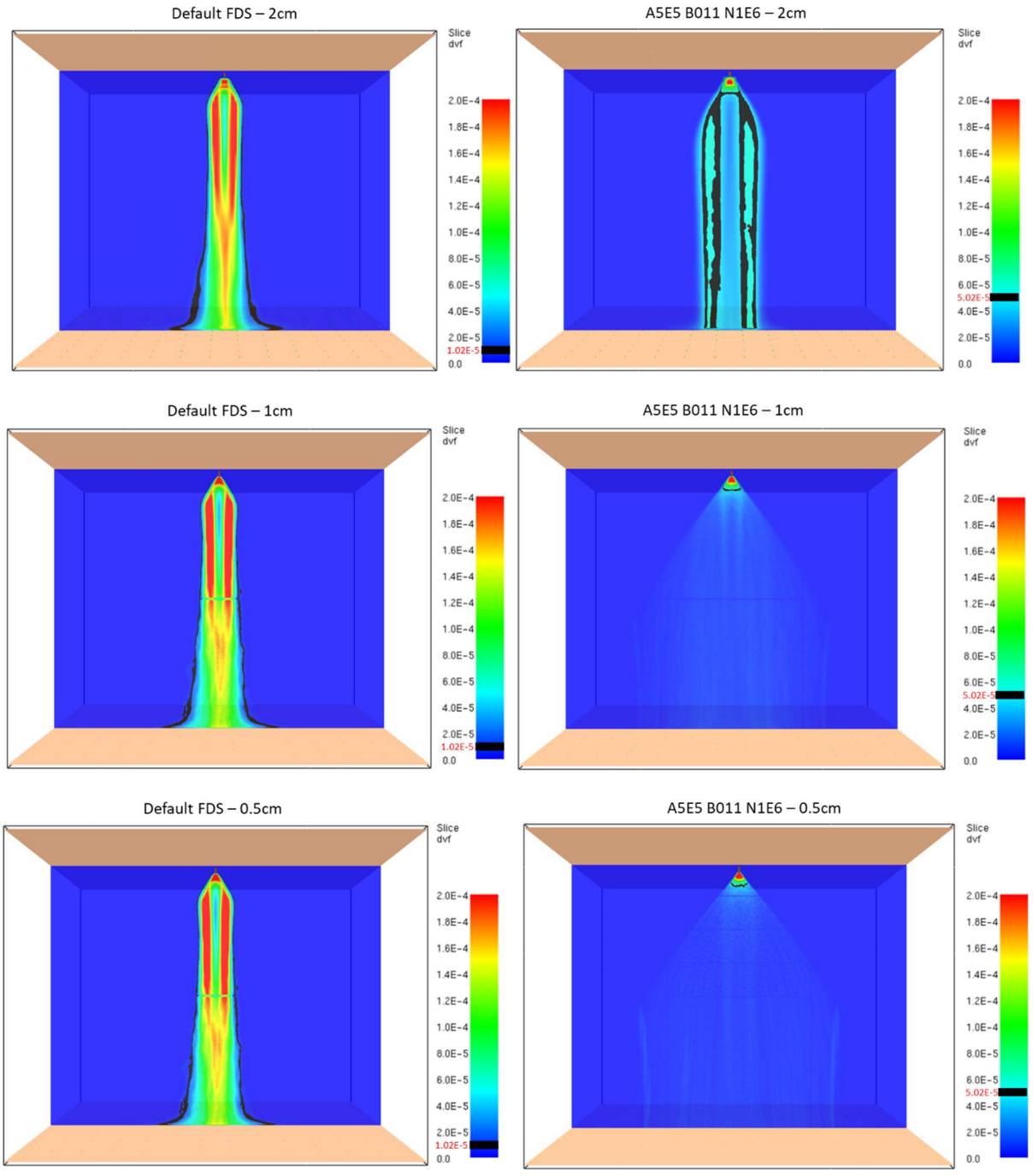

Figure 14 – Comparison of the time averaged (on a period of 5s) droplet volume fraction for the default FDS simulation (left) and the $A = 5 \times 10^{-5}, B = 0.11$ & $n = 10^{-6}$ simulations for different mesh configurations

It is important to mention that, strictly speaking, convergence is not reached for the coarser mesh. Indeed, in simple gas phase simulations, the convergence will be reached by refining the mesh : beyond a certain grid size, the simulations results will be mesh unsensitive and the convergence will be reached for the numerical simulations. For such a complex two-phase flow simulation, the convergence is less

straightforward. This is actually a general problem that pertains to Lagrangian–Eulerian simulations. In 2006, Schmidt stated that if the number of computational particles does not increase while the cell size is reduced, the mean expected error increases after having reached an optimum [27]. As shown by Schmidt et al. [28], the most challenging part in the Lagrangian-Eulerian computation is the 'liquid to gas coupling', or in other words, the accumulation of the mass, momentum, energy and species contributions of the dispersed particles on the source terms in the gas phase equations. As a consequence of the limited number of tracked particles, there is a statistical uncertainty in the source terms.

A mesh refinement will reduce the spatial error. However, if this mesh refinement is realized without increasing the number of computational particles, the statistical error may increase as the latter one is inversely proportional to the cell size [28].

Therefore, an inadequate mesh refinement for spray modelling may alter the quality of the simulation results. For simplified situations, Schmidt et al. have tried to provide some guidance on how the number of particles must be increased with the mesh refinement in order to obtain convergence [28]. However, the case at hand is out of the scope of Schmidt's paper as it is even more complex. Unfortunately, at the moment, there not a rule that provides the correct N_p that should be imposed for such complex simulations to be sure to avoid those statistical errors. This is also the reason why the injection rate of super droplet has been set to a higher value than the default one in FDS but, the authors may not guarantee that the optimum (from both a point of view of mesh size and N_p) has been reached to get full numerical convergence (i.e., a mesh unsensitive solution and unsensitive solution regarding the N_p). Based on the available computational resource for this study and on the fact that this optimum could not be guaranteed, it has been decided not to further increase the injection rate (that has already been multiplied by 40 compared to its default value). It is worth mentioning that the intention of this paper is to present the novel DVF-based drag reduction model and the 'novel' engineering approach that has been used to calibrate this model.

Despites the difference between the curves of the flow rate at the ground on Figure 13, it is important to mention that total flow rate collected at the ground is very close to the imposed flow rate of $1\ L/min$. Indeed, for all the default FDS simulations, it is around $0.98 L/min$ which lead to a relative deviation of 2%. For the novel model, it is $1.01\ L/min$, $0.93\ L/min$ and $0.92\ L/min$ for, respectively, the 2 cm, the 1 cm and the 0.5 cm simulations. This lead thus to a relative difference of -1%, 7% and 8%. The explanation for those differences may be found in the water mass balance: when the mesh is refined, the averaged (on the 8 last seconds) water mass loss rate increases from 0.05 L/min for the coarser mesh to, respectively, 0.10 and 0.11 L/min for the 1 cm and 0.5 cm configurations.

In the absence of more experimental data for the spray at hand, based on previous analysis and based on the potential increase for the statistical error, it may be assumed that the finest mesh refinement (and its possible positive effect on the gas phase) is not sufficient to warrant the increased computational cost. Furthermore, the novel model (through the choice of its parameters) seems to be sensitive to the cell size. Some effort should be done in the future on the convergence of such simulations. Some extra work is also necessary to further consolidate the present DVF-based drag reduction model.

4. Assessment of the novel DVF-based drag reduction model to other water sprays

In order to further assess the influence of the proposed drag reduction model on water sprays, two extra sets of data are considered here. The first one is the LN-2 spray nozzle experimentally and numerically investigated by Vaari et al [29] and Ditch et al. [17]. This case is also referred to in the FDS Validation Guide

[18] as the 'VTT Water Spray' and is available on the FDS' GitHub page [30]. It is more dilute than the Wuhan spray. The second one is the Fukui spray that is described in [19], also expected to be more dilute than the Wuhan spray.

4.1. VTT water spray

In [17], the following spray specifications are given: a volume median diameter of 79 µm, a water flow rate of 0.348 L/min and a discharge pressure of 2068 kPa. This generates a full cone spray pattern whose spray angle is $60° \pm 10°$. Different measurement techniques were used, like the Phase Doppler Particle Analyzer (PDPA) [17] and the Direct Imaging (DI) Shadowgraphy [29]. This provides a data set where, a.o., the size distribution and the mist flux at several locations is known.

The computational domain is a rectangular box (1.0 m x 1.0 m x 1.5 m) with all the boundaries set to 'OPEN'. The nozzle head is positioned 20 cm below the top boundary. A cubic cell size of 2 cm or 1 cm is taken. This is not enough in terms of convergence because, as mentioned in [29], even with a spatial resolution of 1 cm, the results do not show convergence for the spray velocity profile. This is related to the convergence problem of the Lagrangian/Eulerian approach mentioned earlier. It was thus decided to keep only the 2 cm and 1 cm (and not the 0.5 cm) spatial discretization for this study, leading to reasonable calculation times.

Careful checking of the FDS input file as available on the GitHub page, reveals that the spray specifications have not entirely been set as would be expected from the experimental characteristics of the spray. For instance, the half-spray angle has been set to 45° because a Gaussian distribution was used with specific parameters that create an hollow cone. Still, in the present paper and based on the experimental description, 30° has been chosen. The flow rate is set to 0.348 L/min. The injection velocity is obtained, based on the discharge pressure, through the equation available in [29]:

$$v_{d,0} = C\sqrt{\frac{2\Delta p}{\rho_d}} \tag{13}$$

where ρ_d is the density of the water and C that is nozzle-dependent is taken as 0.95 to account for the friction losses in the nozzle. This gives an initial droplet velocity of 60 m/s. A Rosin-Rammler-lognormal distribution with a volume-median diameter, $D_{V,0.50}$, of 79 µm and a spread factor, γ_D, of 2.1 is taken for the drop size distribution. The mass flux distribution at the injection boundary (0.08 m from the nozzle) is set to be 'UNIFORM' as for the 'Wuhan' spray simulations. The VTT spray is less dense than the one studied before, therefore it is decided to take a smaller number of tracked particles. Every second, $100\,000$ computational droplets are injected, which is also the number that was chosen in the input file available on [30].

Figure 15 shows different water mist flux predictions. The first set, in blue, are the numerical results that are obtained with the default version 6.7.6 of the FDS code and will serve as point of comparison for the novel DVF-based drag model results. For the default simulation, the mist flux is under-predicted compared to the experimental data. At the center of the spray, this leads to a relative underestimation of 17% and 22% for, respectively, the $\Delta x = 2$ cm and $\Delta x = 1$ cm simulations. The mesh sensitivity of the results is weak, as was the case for the Wuhan spray (Figure 13).

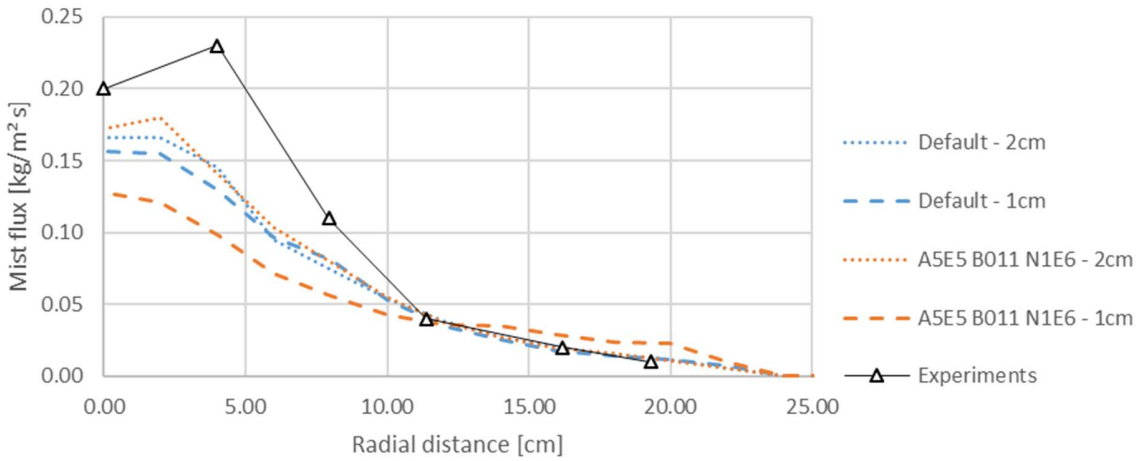

Figure 15 – The mist flux for the VTT spray at 40 cm from the nozzle for the default FDS simulations, the novel model $A = 5 \times 10^{-5}, B = 0.11$ & $n = 10^6$ and the experiments [29]

The simulations with the novel DVF-based drag reduction model, in orange, reveal that the differences between the default FDS simulations and the novel approach are much smaller than for the Wuhan spray on the fine meshes. This was expected as the VTT spray is less dense than the Wuhan spray. The novel model was built to improve the drag prediction of very dense regions but without affecting too simulation results for less dense sprays (Figure 2). As in the Wuhan spray, the results with the novel model are more sensitive to the mesh than the default FDS simulations.

4.2. Simulation results for the Fukui spray

The Fukui spray [19] is also expected to be more dilute than the Wuhan spray. Indeed, even if the half spray angle is only 28°, the volume flow rate is much smaller, i.e. $0.439\ L/min$, and the droplets are larger in size, i.e., a volume median diameter of $258.2\ \mu m$. The operating pressure is around $0.246\ MPa$ and the orifice diameter is $0.69\ mm$. The ejection velocity from the nozzle, obtained from Eq. (16), is $21\ m/s$. The water flow rate, in the absence of the fire source, has been measured with buckets placed 1 m below the nozzle. The droplet size distribution has been determined from pictures from microscope camera: a Rosin-Rammler-lognormal distribution with a spread factor, γ_D, of 3.2 is taken.

The computational domain is again a rectangular box (1.6 m x 1.6 m x 1.64 m) and all the boundaries are set to 'OPEN'. The nozzle head is positioned 336 mm below the top boundary. Two mesh configurations with identical cubic cells have been investigated: a 16 mm and a 8 mm cell size. An offset of $0.032m$ has been chosen with a Gaussian distribution. The number of particles inserted into the simulation domain per second is 50 000 (as done in [19]), which is 10 times higher than the default value in FDS.

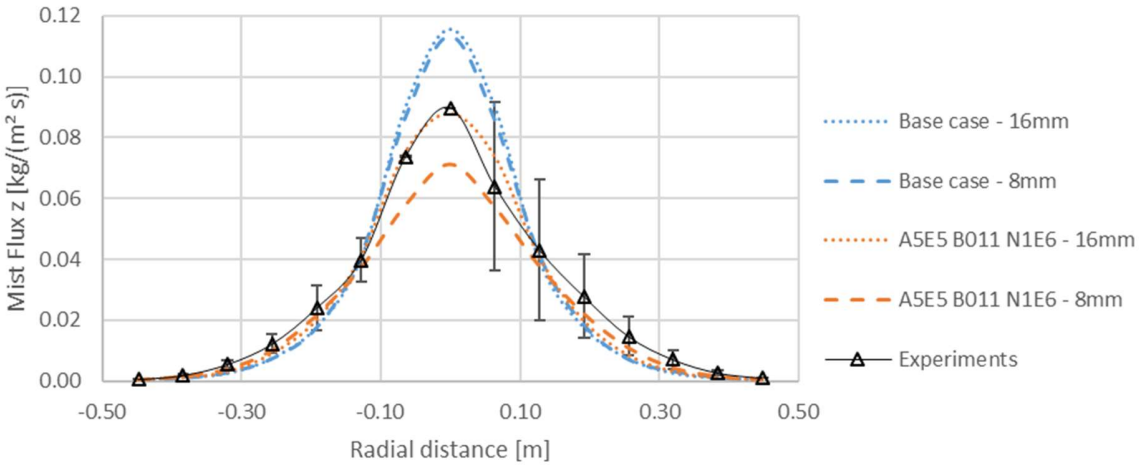

Figure 16 – Water mist flux at 1 m from the nozzle for the Fukui spray for the FDS default simulations, the novel model $A = 5 \times 10^{-5}, B = 0.11$ & $n = 10^6$ and the experiment results from [19]

As before, the default FDS (version 6.7.6) simulation results serve as a point of comparison. Figure 16 reveals very little mesh sensitivity for the mist flux at 1 m from the nozzle, over-predicting the measurement data. The DVF-based drag reduction model (with $A = 5 \times 10^{-5}, B = 0.11$ & $n = 10^6$) yields a mist flux profile that matches the measurements very closely on the $\Delta x = 16\,mm$ mesh. However, refining the mesh ($\Delta x = 8\,mm$) reveals mesh sensitivity and leads to an under-prediction of the experiments, as for the VTT spray.

5. Discussion

For the sake of further reflection, it is worth mentioning that the proposed set of parameters A, B & n should not be considered as the final set that should be universally used. This paper only intends to present a novel approach that needs to be further investigated (e.g., the convergence difficulty) and should be assessed against more experimental data at several positions in the spray.

For instance, another set of parameters, $A = 10^{-5}, B = 0.11$ and $n = 10^6$ (green curve in Figure 1) provides even better results for the Wuhan spray, but deteriorates the agreement for the two other sprays. This set has a lower value for the parameter A. As a consequence, the drag reduction will occur for lower α values, so the drag will be reduced even for more dilute regions than compared to the set of parameters above. The corresponding water flux density is shown in Figure 17. This time, the best simulation results are obtained for the $2\,cm$ mesh configuration. However, when the mesh is refined, the curves show that, although the results are better than the default FDS simulations in Figure 13, the flux density is too flat compared to the experimental results.

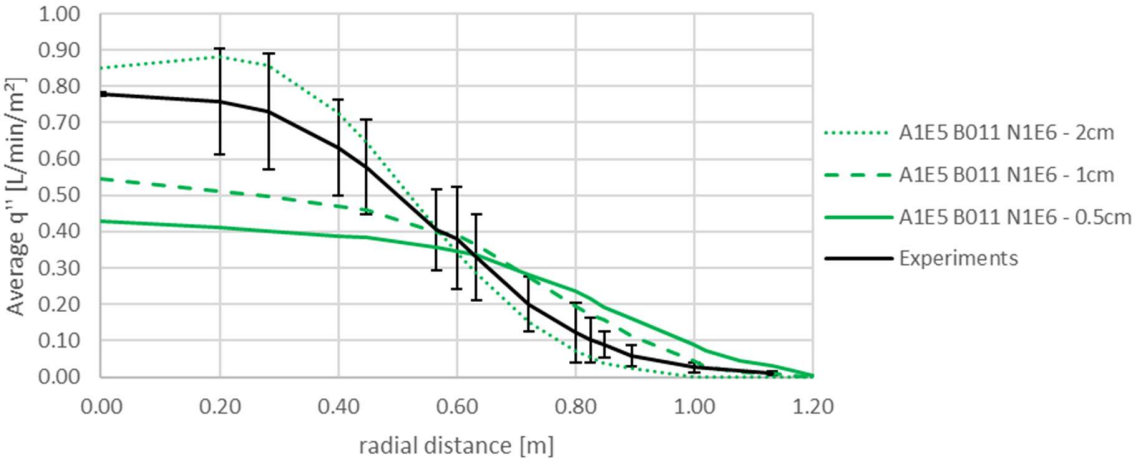

568

569 Figure 17 – The water flux density distribution along the radial direction for the Wuhan spray for the novel model
570 drag reduction simulation with a second set of parameters ($A = 10^{-5}, B = 0.11, n = 10^{6}$) and the experiments

571 However, the excessive drag reduction for $10^{-5} \leq \alpha \leq 5.10^{-5}$ worsens the results for the VTT and Fukui
572 sprays (Figure 18). Interestingly, the results do become less mesh sensitive, because the region where α
573 has a value close to where the drag reduction changes rapidly from almost no drag reduction ($\alpha \leq 10^{-5}$)
574 to full drag reduction is less in a critical region of the spray.

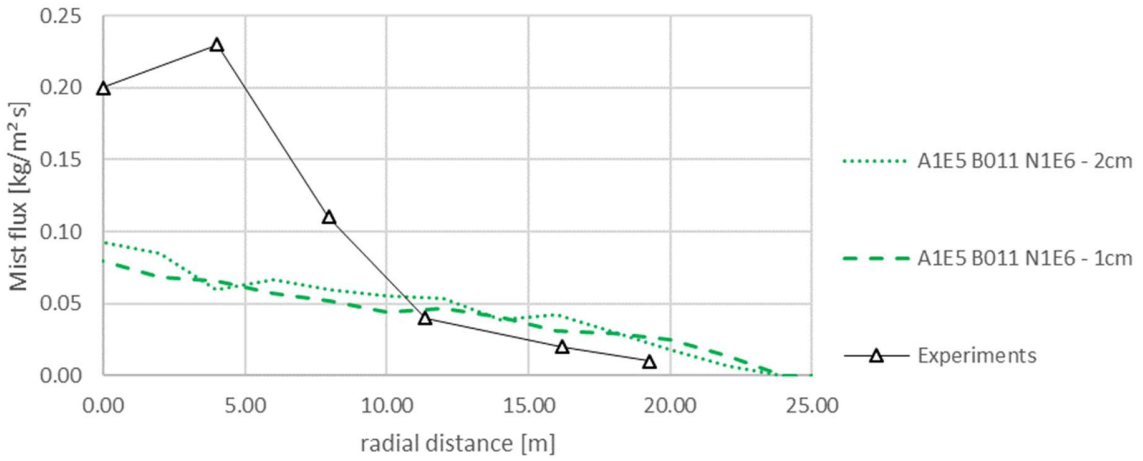

575

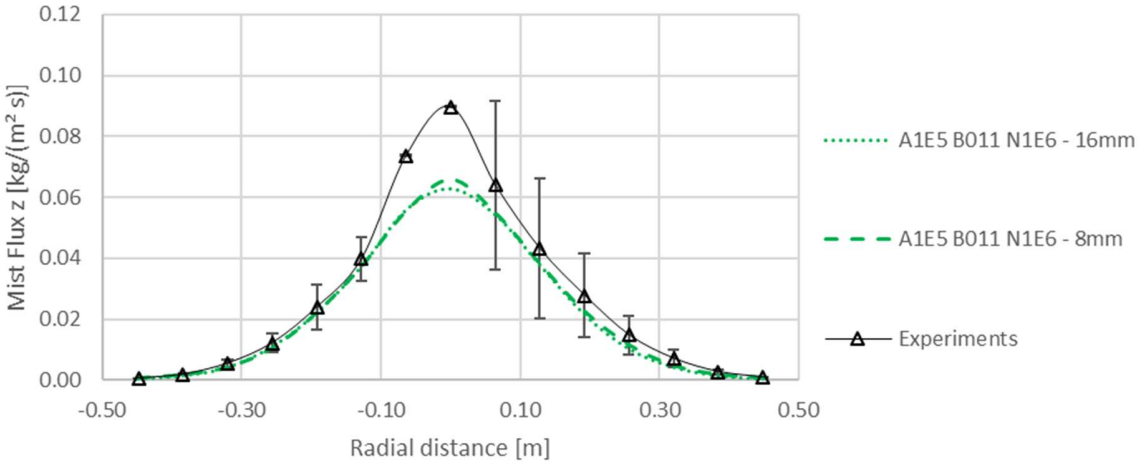

576

577 Figure 18 – The mist flux for the VTT spray at 40 cm from the nozzle (top) and for the Fukui spray (bottom) for the
578 novel model ($A = 10^{-5}, B = 0.11$ & $n = 10^{6}$) simulations and the experiments results

579 Therefore, one should be careful when choosing a specific set of parameters, because if it provides good
580 results for one range of spray (in terms of density) it may worsen the simulation results for other sprays.
581 Further investigation on this is considered future work.

582 ## 6. Conclusions

583 This paper proposes a novel approach to model the drag reduction correction that has then been
584 compared to different water sprays. The newly developed drag correction function shows – for very dense
585 sprays – that by substantially reducing the drag force in dense regions of the spray, typically near the
586 nozzle, this will have a large impact on the spray envelope of the spray. The spray expands more near the
587 injection. This provides simulation results that better reproduce the experimental spray. Still, in the
588 regions of the spray that are very dilute, the function does not reduce the drag modelling which is
589 coherent with the reality. The novel DVF-based drag correction formulation may lead to better water flux
590 distribution at the ground. However, the results with the novel expression have shown to be very sensitive
591 to the cell size which is something to investigate more in the future.

The model has been applied to 3 sprays with variable levels of diluteness and the model parameters (A, B and n) can be adjusted to optimize agreement. However, the optimum values depend on the case and on the mesh used. The model needs to be assessed against more well-documented experimental datasets or DSN type numerical simulations in order to gain more insight when applied to different sprays, on a range of computational meshes. Therefore, the present combination of model parameter values may not be regarded as definitive now.

Acknowledgments

Martin Thielens is a PhD student who holds a grant for fundamental research from the Fund of Scientific Research – Flanders (FWO – Vlaanderen). The FWO file number of his mandate is 1182919N.

Statements and Declarations

The authors declare that are no financial or non-financial conflicts of interests.

Author contribution

All authors contributed to the study conception and design. Material preparation, data collection and analysis were performed by Martin Thielens, Tarek Beji and Yuanjun Liu. The first draft of the manuscript was written by Martin Thielens and all authors commented on previous versions of the manuscript. The paper has been deeply reviewed by Tarek Beji and Bart Merci. All authors read and approved the final manuscript.

7. References

[1] G. G. Stokes, "On the Effect of Internal Friction of Fluids on the Motion of Pendulums," *Transaction of the Cambridge Philosophical Society,* vol. 9, no. 2, pp. 8-106, 1851.

[2] M. Sommerfeld, B. Van Wachem and R. Oliemans, Best Practice Guidelines for Computational Fluid Dynamics of Dispersed Multiphase Flows, European Research Community On Flow Turbulence And Combustion, 2008.

[3] C. E. Lapple and C. B. Shepherd, "Calculation of Particle Trajectories," *Ind. Eng. Chem.,* vol. 32, pp. 605-617, 1940.

[4] R. Clift, J. R. Grace and M. E. Weber, Bubbles, Drops, and Particles, Academic Press, 1978.

[5] L. Schiller and A. Z. Naumann, "Über die Grundlegenden Berechnungen bei der Schwerkraftaufbereitung," *Ver. Deut. Ing,* no. 77, pp. 318-320, 1933.

[6] J. Happel and R. Pfeffer, "The Motion of Two Spheres FOllowing Each Other in a Viscous Fluid," *A.I.C.H.E Journal,* vol. 6, no. 1, pp. 129-133, 1960.

[7] C. H. Chiang and W. A. Sirignano, "Axisymmetruc Calculations of Three-Droplet Interactions," pp. 1-12, 1992.

[8] S. Elghobashi, "On Predicting Particle-Laden Turbulent Flows," *Applied Scientific Research,* vol. 52, pp. 309-329, 1994.

[9] M. Salewski and L. Fuchs, "Effects of Aerodynamic Particle Interaction in Turbulent Non-Dilute Particle-Laden Flow," *Journal of Turbulence,* vol. 9, no. 46, pp. 1-23, 2008.

[10] K. McGrattan, S. Hostikka, R. McDermott, J. Floyd and M. Vanella, "Fire Dynamics Simulator Technical Reference Guide Volume 1: Mathematical Model, Sixth Edition," National Institute of Standards and Technology, 2019.

[11] J. Ramírez-Muñoz, A. Soria and E. Salinas-Rodríguez, "Hydrodynamic force on interactive spherical particles due to the wake effect," *International Journal of Multiphase Flow,* vol. 33, no. 7, pp. 802-807, 2007.

[12] C. Zhu, S.-C. Liang and L.-S. Fan, "Particle Wake Effects on the Drag Force of an Interactive Particle," *Int. J. Multiphase Flow,* vol. 20, no. 1, pp. 117-129, 1994.

[13] L. Prahl, A. Hozler, D. Arlov, J. Revstedt, M. Sommerfeld and L. Fuchs, "On the interaction between two fixed spherical particles," *International Journal of Multiphase Flow,* vol. 33, pp. 707-725, 2007.

[14] K. McGrattan, S. Hostikka, R. McDermott, J. Floyd, C. Weinschenk and K. Overholt, Fire Dynamics Simulator User's Guide, 6th Edition, NIST, 2019.

[15] I. Silverman and W. A. Sirignano, "Multi-Droplet Interaction Effects in Dense Sprays," *Int. J. Multiphase Flow,* vol. 20, no. 1, pp. 99-116, 1994.

[16] Y. Liu, T. Beji, M. Thielens, Z. Tang, Z. Fang and B. Merci, "Numerical Analysis of a Water Mist Spray: the Importance of Various Numerical and Physical Parameters, Including the Drag Force," *Fire Safety Journal,* vol. 127, p. 103515, 2022.

[17] B. Ditch and H.-Z. Yu, "Water Mist Spray Characterization and its Proper Application for Numerical Simulations," *Fire Safety Science,* no. Proceedings of the Ninth International Symposium, pp. 541-552, 2008.

[18] K. McGrattan, S. Hostikka, R. McDermott, J. Floyd and M. Vanella, Fire Dynamics Simulator Technical Reference Guide Volume 3: Validation, Sixth Edition, National Institute of Standards and Technology, 2021.

[19] S. Noda, B. Merci, F. Tanaka and T. Beji, "Experiments and Numerical Study on the Interaction of a Water Mist Spray with a Turbulent Buoyant flame," *Fire Safety Journal,* no. 120, 2021.

[20] H. Rusche and R. Issa, "The Effect of Voidage on the Drag Force on Particles, Droplets and Bubbles in Dispersed Two-Phase Flow," Proceedings of the 2nd Japanese-European Two-Phase Flow Group Meeting, Tsukuba, Japan, 2000.

[21] M. Takagi and Y. Moriyoshi, "Application of Drag Rudction Model Accounting for Droplet Number Density to a Diesel Spray," *Transactions of the Japan Society of Mechanical Engineers,* pp. 272-278, 2008.

[22] D. D. McClure, J. M. Kavanagh, D. F. Fletcher and G. W. Barton, "Experimental invetsigation into the drag volume fraction correction tems for gas-liquid bubbly flows," *Chemical Engineering Science,* vol. 170, pp. 91-97, 2017.

[23] S. S. Rabha and V. V. Buwa, "Experimental Investigations of Rise Behavior of Monodispersed/Polydispersed Bubbly Flows in Quiescent Liquids," *Industrial and Engineering Chemistry Research,* no. 49, pp. 10615-10626, 2010.

[24] A. Naumann, "Luftwiderstand von Kugeln bei hohen Unterschallgeschwindigkeiten," *Allgem. Wärmetechnik.,* vol. 4, pp. 217-221, 1953.

[25] NFPA, "NFPA 750, Standard on Water Mist Fire Suppression Systems," National Fire Protection Association, Quincy, MA, 1996.

[26] T. Sikanen, J. Vaari, S. Hostikka and A. Paajanen, "Modeling and Simulation of High Pressure Water Mist Systems," *Fire Technology,* vol. 3, no. 50, pp. 483-504, 2014.

[27] D. P. Schmidt, "Theoritical Analysis for Achieving High-order Spatial Accuracy in Lagrangian/Eulerian Source Terms," *International Journal for Numerical Methods in Fluids,* vol. 52, no. 8, pp. 843-865, 2006.

[28] D. P. Schmidt and F. Bedford, "An Anlysis of the Convergence of Stochastic Lagrangian/Eulerian Spray Simulations," *International Journal of Multiphase Flow,* no. 102, pp. 95-101, 2018.

[29] J. Vaari, S. Hostikka, T. Sikanen and A. Paajanen, "Numerical Simulations on the Performance of Water-Based Fire Suppression Systems," VTT Technology 54, Finland, 2012.

[30] "Fire Dynamics Simulator: GitHub page," [Online]. Available: https://github.com/firemodels/fds/tree/master/Validation/VTT_Sprays/FDS_Input_Files. [Accessed 27 10 2021].

614